3-bar tensegrity units with non-equilateral triangle on an end plane

AUTHOR(S):

Liu, Heping; Zhang, Jingyao; Ohsaki, Makoto

CITATION:

Liu, Heping ...[et al]. 3-bar tensegrity units with non-equilateral triangle on an end plane. Mechanics Research Communications 2018, 92: 124-130

ISSUE DATE:

2018-09

URL:

http://hdl.handle.net/2433/236124

Submitted to Mechanical Research Communications

3-bar tensegrity units with non-equilateral triangle on an end plane

Heping Liu[1,3*], Jingyao Zhang[2] and Makoto Ohsaki[1]

[1] *Department of Architecture and Architectural Engineering, Kyoto University, Kyoto-Daigaku Katsura, Nishikyo, Kyoto 615-8540, Japan*
[2]*Graduate School of Design and Architecture, Nagoya City University, 2-1-10, Kita Chikusa, Chikusa-ku, Nagoya 464-0083, Japan*
[3] *College of Mechanical and Electrical Engineering, Harbin Engineering University, Harbin 150001, China*
*liuheping@hrbeu.edu.cn
Tel.:+86-0451-82519710; fax: +86-0451-82519710

Abstract

The well-known 3-bar prismatic tensegrity unit has equilateral triangles on the two end planes. In this paper, properties of the 3-bar tensegrity unit with non-equilateral triangle on one end plane are investigated. The unit is generated by transforming the equilateral triangle of the tensegrity prism to a triangle with irregular shape. The self-equilibrium equations of the 3-bar tensegrity unit are analytically solved for geometrical parameters and force densities of the members. The analytical solutions are utilized to investigate detailed characteristics of the 3-bar tensegrity units with non-equilateral triangle on an end plane.

[Graphical Abstract]

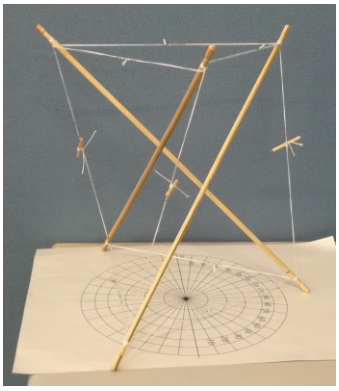

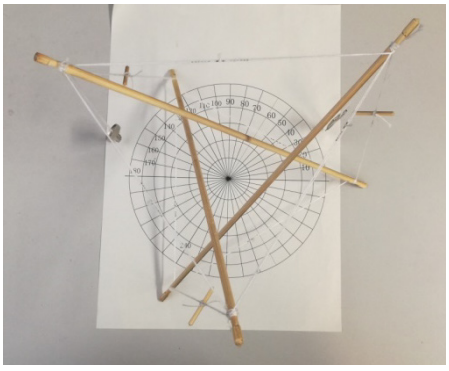

Keywords: 3-bar tensegrity unit, non-equilateral triangle, equilibrium equation, analytical solution, geometrical parameters, force densities.

1. Introduction

Tensegrity structures are self-equilibrated frameworks composed of bars in compression and strings in tension [1-3]. Because of their lightweight, shape control and tunable stiffness properties, they have received interests in many fields including architecture, civil engineering, aerospace, robotics, sculpture and biology [4-8]. Some novel tensegrity structures have been developed to further broaden their applications.

Form finding by using optimization can generate novel tensegrity structures and can obtain required geometric shapes with excellent mechanical properties; therefore, more and more researchers have paid their attention to optimization methods. Lee et al. [9] minimized fitness functions by using a double-loop genetic algorithm in the form-finding process. A well-known truncated tetrahedral tensegrity was presented to demonstrate the accuracy and efficiency of the proposed method. Ohsaki and Zhang [10] presented an optimization approach to form-finding and folding analysis of tensegrity structures using fictitious material properties. It was demonstrated that various equilibrium shapes can be easily found by solving a forced-deformation analysis problem formulated as a minimization problem of an energy function.

The method of assembling tensegrity units together as cells into various geometrical shapes is also commonly used. Fraddosio et al. [11] investigated V-Expanders, which are elementary cells for a tensegrity mast for a MoMA exhibition. Spisaka and Kmet [12] presented a tensegrity girder composed of 5-strut tensegrity pyramids. A non-linear static analysis was utilized to find optimal length modifications of active members. Nagase et al. [13] provided a systematic way to construct connectivity matrices for tensegrity structures from repetition of tensegrity prisms. They focused on double-helix tensegrities consisting of units aligned along their axes to build some spatial shapes such as tori, cylinders, paraboloids, and spheres. Lu et al. [14] assembled semi-regular tensegrity units in the torus and then generated a novel cable–strut tensile structural system through combining a tensegrity torus and a Levy-type cable dome. Liu et al. [15] investigated the method for connecting tensegrity units along their axes to set up cylindrical and circular tensegrity structures. The tensegrity ball, which has been applied as framework of the ball tensegrity robot by NASA, is composed of two 3-bar tensegrity units [16-18].

Simple tensegrity structures are widely used as elementary units to assemble complicated structures [11]. Generation of various types of tensegrity units can contribute to obtaining more different types of tensegrity structures. So it is important to develop a method for generating various types of tensegrity units, and to investigate characteristics of the units. The well-known 3-bar prismatic tensegrity unit is a typical tensegrity unit, so the 3-bar prismatic tensegrity unit will be studied in this paper. Numerical methods, for example optimization methods [15], require much higher computational time than analytical methods. Hence, analytical methods are preferable, as long as they are applicable to find the self-equilibrated shapes of tensegrity structures. Rather than numerical methods, analytical solutions provide a direct way to investigate the relations between the parameters. So this paper will focus on analytical solutions of the structural parameters.

In the reference [19], additional strings were added to the well-known 3-bar tensegrity unit, where the triangles at the two ends were kept regular. To have more control over the self-equilibrated shape, we consider in this paper a different problem of finding analytical solutions for the 3-bar prismatic tensegrity unit with irregular triangle at one of the two ends. The properties of new units are investigated analytically based on the equilibrium equations with respect to the force densities. Relation between the force and geometry as well as the limitations in the configurations are explicitly derived based on the analytical expressions.

2. Basic problems

Figure 1(a) shows the 3-bar prismatic tensegrity unit, which is composed of three bars and nine strings. Its members can be classified into four kinds; namely, bars, declining strings, top level strings and bottom level strings. Every kind of members has the same length. The two end planes are parallel to each other. Level strings on each end plane are the edges of an equilateral triangle. Equilibrium of the unit with the regular configuration is dependent on θ_1 only, which is the angle projected on the bottom plane and rotated from node 1 to node 4 as shown in Fig. 1(a). Note that node i is sometimes indicated as n_i below to

distinguish it from other indices as member numbers. The height is H, and the three nodes on the top and bottom planes, respectively, are located along the circles of radius r_1 and r_2.

When the two end planes of the prismatic tensegrity units are regular polygons, the angle θ_1 must satisfy [20]

$$\theta_1 = \frac{\pi}{2} + \frac{j\pi}{p}, \quad (j = 1, \ldots, p-1) \tag{1}$$

where p is the number of bars in the tensegrity unit. Therefore, when the 3-bar prismatic tensegrity unit is self-equilibrated, θ_1 must be equal to 150° or 210°. The two units are distinguished by connection of declining strings. Figure 1 shows the tensegrity unit when θ_1 is equal to 150°, where nodes 1, 2 and 3 are connected to nodes 6, 4 and 5, respectively. In the tensegrity unit with θ_1=210°, nodes 1, 2 and 3 are connected to nodes 5, 6 and 4, respectively, by declining strings. Moreover, the nodes and members of the structures with different θ_1 are symmetric with respect to xz-plane. In this paper, we generate various irregular shapes from the tensegrity unit with θ_1=150°.

Figure 1(b) shows projections of nodes 4, 5 and 6 on the bottom plane. We investigate the self-equilibrated shape when the polygon formed by the three nodes is not an equilateral triangle. In Fig. 1(b), θ_2 and θ_3 are the angles projected on the bottom plane and rotated from node 1 to nodes 5 and 6, respectively.

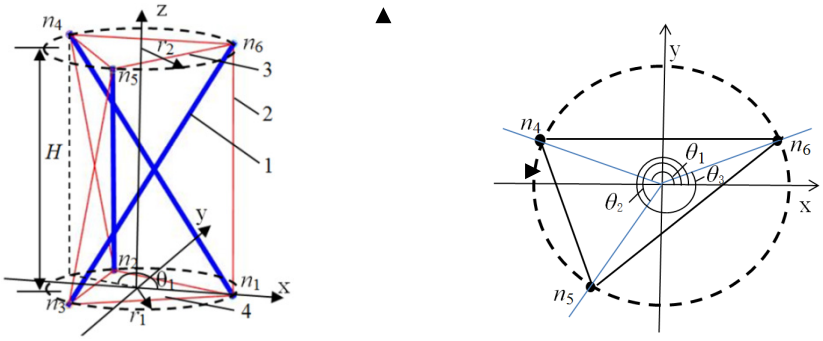

(a) (b)

Fig.1. 3-bar tensegrity unit with θ_1=150°; 1: bars, 2: declining strings, 3: top level strings, 4: bottom level strings; (a) diagonal view, (b) plan view.

Numerical approaches can be applied to find equilibrium shape of a tensegrity structure with irregular shape. However, it is difficult to investigate the detailed characteristics of the shape numerically. By contrast, analytical solutions of structural parameters can explicitly reflect relations between the parameters, and can be applied easily to obtain various new configurations. Tibert and Pellegrino [21] obtained equilibrium conditions for the well-known prismatic tensegrity units by solving equilibrium equations in symbolic form. In this study, we derive analytical solutions for irregular tensegrity units.

Before analysis, we suppose:

1) The two end planes are parallel with each other;
2) The polygon consisting of nodes 1, 2 and 3 is an equilateral triangle;
3) Nodes 4, 5 and 6 are placed on the circle as shown in Fig. 1(b) with radius different from nodes 1, 2 and 3;
4) The relation $\theta_1<\theta_2<\theta_3$ is always satisfied;
5) Connectivity between members and nodes is the same as the tensegrity unit in Fig. 1(a);
6) No external load is considered in self-equilibrium analysis.

3. Self-equilibrium analysis

Connectivity between the nodes and members are listed in Table 1, where the first three members are bars and the other members are strings.

Table 1. Connectivity between the nodes and members.

Member	Starting node	Ending node
1	1	4
2	2	5
3	3	6
4	1	2
5	2	3
6	3	1
7	4	5
8	5	6
9	6	4
10	1	6
11	2	4
12	3	5

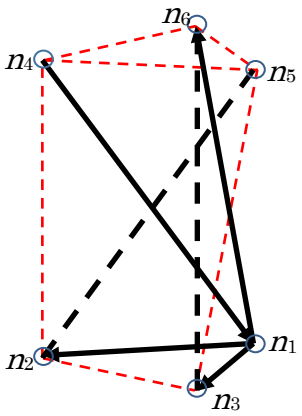

Fig. 2. Force equilibrium at node 1.

The equilibrium equations are formulated with respect to the force densities. Let L_i and F_i denote the length and axial force of member i, respectively. The force density q_i is defined as the ratio of force to length as $q_i=F_i/L_i$. Figure 2 shows force equilibrium at node 1. Let r_1, r_2 and H denote the radii of bottom and top circles and the height, respectively. We use a symbolic computation software package Maple 2016 [22] to assist analytical derivation of equations. According to Fig. 3, equilibrium equations in x-, y- and z-directions at node 1 can be expressed with respect to the force densities as

$$\begin{cases} \left(q_1+\frac{3}{2}q_4+\frac{3}{2}q_6+q_{10}\right)r_1-q_1r_2\cos\theta_1-q_{10}r_2\cos\theta_3=0 \\ -\frac{\sqrt{3}}{2}q_4r_1+\frac{\sqrt{3}}{2}q_6r_1-q_1r_2\sin\theta_1-q_{10}r_2\sin\theta_3=0 \\ -Hq_1-Hq_{10}=0 \end{cases} \tag{2}$$

Similarly to node 1, equilibrium equations at other nodes can be written as

$$\text{Node 2:}\begin{cases} -\frac{1}{2}(q_2+3q_4+q_{11})r_1-q_{11}r_2\cos\theta_1-q_2r_2\cos\theta_2=0 \\ \frac{\sqrt{3}}{2}(q_2+q_4+2q_5+q_{11})r_1-q_{11}r_2\sin\theta_1-q_2r_2\sin\theta_2=0 \\ -Hq_2-Hq_{11}=0 \end{cases} \tag{3a}$$

$$\text{Node 3:}\begin{cases} -\frac{1}{2}(q_3+3q_6+q_{12})r_1 - q_{12}r_2\cos\theta_2 - q_3r_2\cos\theta_3 = 0 \\ -\frac{\sqrt{3}}{2}(q_3+2q_5+q_6+q_{12})r_1 - q_{12}r_2\sin\theta_2 - q_3r_2\sin\theta_3 = 0 \\ -Hq_3 - Hq_{12} = 0 \end{cases} \tag{3b}$$

$$\text{Node 4:}\begin{cases} -q_1r_1 + \frac{1}{2}q_{11}r_1 + (q_1+q_7+q_9+q_{11})r_2\cos\theta_1 - q_7r_2\cos\theta_2 \\ -q_9r_2\cos\theta_3 = 0 \\ -\frac{\sqrt{3}}{2}q_{11}r_1 + (q_1+q_7+q_9+q_{11})r_2\sin\theta_1 - q_7r_2\sin\theta_2 \\ -q_9r_2\sin\theta_3 = 0 \\ Hq_1 + Hq_{11} = 0 \end{cases} \tag{3c}$$

$$\text{Node 5:}\begin{cases} \frac{1}{2}q_2r_1 + \frac{1}{2}q_{12}r_1 - q_7r_2\cos\theta_1 + (q_2+q_7+q_8+q_{12}) \\ r_2\cos\theta_2 - q_8r_2\cos\theta_3 = 0 \\ -\frac{\sqrt{3}}{2}q_2r_1 + \frac{\sqrt{3}}{2}q_{12}r_1 - q_7r_2\sin\theta_1 + (q_2+q_7+q_8+q_{12}) \\ r_2\sin\theta_2 - q_8r_2\sin\theta_3 = 0 \\ Hq_2 + Hq_{12} = 0 \end{cases} \tag{3d}$$

Node 6:

$$\begin{cases} -q_{10}r_1 + \frac{1}{2}q_3r_1 - q_9r_2\cos\theta_1 - q_8r_2\cos\theta_2 + \\ (q_3+q_8+q_9+q_{10})r_2\cos\theta_3 = 0 \\ \frac{\sqrt{3}}{2}q_3r_1 - q_9r_2\sin\theta_1 - q_8r_2\sin\theta_2 + \\ (q_3+q_8+q_9+q_{10})r_2\sin\theta_3 = 0 \\ Hq_3 + Hq_{10} = 0 \end{cases} \tag{3e}$$

From the third equilibrium equations of all the nodes, we can easily obtain

$$\begin{aligned} q_1 &= q_2 = q_3 \\ q_{10} &= q_{11} = q_{12} = -q_3 \end{aligned} \tag{4}$$

It is observed from Eq. (4) that the force densities of bars and declining strings have the same absolute value. After solving the second equilibrium equations of Eq. (2) and (3a-e) for all the nodes, the following relations of force densities can be derived:

$$\begin{aligned} q_5 &= \frac{\sqrt{3}q_3r_2(\sin\theta_2 - \sin\theta_1)}{3r_1} - \frac{q_4}{2} \\ q_6 &= q_4 + \frac{2\sqrt{3}q_3r_2(\sin\theta_2 - \sin\theta_3)}{3r_1} \\ q_7 &= \frac{2q_9r_2\sin\theta_3 - 2q_9r_2\sin\theta_1 - \sqrt{3}q_3r_1}{2r_2(\sin\theta_1 - \sin\theta_2)} \\ q_8 &= \frac{\sqrt{3}q_3r_1 + 2q_9r_2\sin\theta_3 - 2q_9r_2\sin\theta_1}{2r_2(\sin\theta_2 - \sin\theta_3)} \end{aligned} \tag{5}$$

From the first equilibrium equations of nodes 1 and 6, we obtain

$$
\begin{aligned}
q_4 &= \frac{q_3 r_2 (\cos\theta_1 - \cos\theta_3 + \sqrt{3}\sin\theta_3 - \sqrt{3}\sin\theta_1)}{3r_1} \\
q_9 &= -q_3 r_1 (\sqrt{3}\cos\theta_1 - \sqrt{3}\cos\theta_2 - 3\sin\theta_2 + 3\sin\theta_1) / \\
&[2r_2 (\cos\theta_2 \sin\theta_1 - \cos\theta_3 \sin\theta_1 - \sin\theta_2 \cos\theta_1 + \sin\theta_4 \cos\theta_1 \\
&- \cos\theta_2 \sin\theta_3 + \cos\theta_3 \sin\theta_2)]
\end{aligned} \tag{6}
$$

The first equilibrium equations of other four nodes are linearly dependent; therefore, only cosine of θ_2 can be solved as

$$
\cos\theta_2 = \frac{1}{2}(\cos\theta_1 + \cos\theta_3) + \frac{\sqrt{3}}{2}(\sin\theta_1 - \sin\theta_3) \tag{7}
$$

Eq. (7) indicates that θ_2 is dependent on θ_1 and θ_3 only; moreover, the three angles are independent of H, r_1 and r_2.

It is well-known that θ_1, θ_2 and θ_3 are equal to 150°, 270° and 390°, respectively, for the 3-bar prismatic tensegrity unit with regular configuration. Substituting 150° and 390° into θ_1 and θ_3 in Eqs. (7), we obtain

$$
\cos\theta_2 = 0 \tag{8}
$$

From Eq. (8), we obtain $\theta_2 = 270°$, which is satisfied by the 3-bar prismatic tensegrity unit; thus, Eqs. (7) has been verified for the special case.

Zhang and Ohsaki [23] showed that there are at least four zero eigenvalues in the force density matrix of the self-equilibrated three-dimensional structures. The force density matrix, denoted by **D**, of the tensegrity unit investigated here can be written as

$$
\mathbf{D} = \begin{bmatrix}
q_1+q_4+q_6+q_{10} & -q_4 & -q_6 & -q_1 & 0 & -q_{10} & -q_1 & 0 & -q_{10} \\
-q_4 & q_2+q_4+q_5+q_{11} & -q_5 & -q_{11} & -q_2 & 0 & -q_{11} & -q_2 & 0 \\
-q_6 & -q_5 & q_3+q_5+q_6+q_{12} & 0 & -q_{12} & -q_3 & 0 & -q_{12} & -q_3 \\
-q_1 & -q_{11} & 0 & q_1+q_7+q_9+q_{11} & -q_7 & -q_9 & -q_7 & q_2+q_7+q_8+q_{12} & -q_8 \\
0 & -q_2 & -q_{12} & -q_7 & q_2+q_7+q_8+q_{12} & -q_8 & -q_9 & -q_8 & q_3+q_8+q_9+q_{10}
\end{bmatrix} \tag{9}
$$

Self-equilibrium of the 3-bar prismatic tensegrity unit is determined by the five parameters; namely, H, r_1, r_2, θ_1 and θ_3, which are mutually independent. If H, r_1 and r_2 are assigned, equilibrium shape is determined only by θ_1 and θ_3 since θ_2 is dependent on θ_1 and θ_3. Here, H is set as 0.25m, r_1 and r_2 are set as 0.1m, for instance. Without loss of any generality, force density of the third bar is given as $q_3 = -1$.

Four cases classified according to the quadrant of xy-plane, where node 4 is located, will be considered; namely, Cases 1, 2, 3 and 4 mean that node 4 is located in the first, second, third and fourth quadrants, respectively. We obtain θ_1, θ_2 and θ_3 of the self-equilibrated configurations using the following procedure:

(1) Firstly, we assign θ_1 and vary θ_3 in the range $[\theta_1, \theta_1 + 360°]$;
(2) Then, Eq. (7) is solved for $\cos\theta_2$ considering which quadrant node 4 exists;
(3) The equilibrium conditions in Section 3 and the fourth condition $\theta_1 < \theta_2 < \theta_3$ in Section 2 are applied further to obtain sets of θ_2 using Eq. (7);
(4) Finally, all geometrical parameters of the self-equilibrated configuration are found from the two of θ_1, θ_2 and θ_3.

4. Properties of the tensegrity unit in Case 1

In Case 1 with $0<\theta_1\leqslant 90°$, it is found that there exists no combination of θ_1, θ_2 and θ_3 for the self-equilibrated configuration when $\theta_1<11°$. Variations of θ_2 and θ_3 are shown in Fig. 3 when θ_1 is varied from 20° to 90°. Note that there are some curves overlapping with each other.

As seen from the figure, with increase of θ_1, ranges of θ_2 and θ_3 become wider. Moreover, when node 4 is located in the first quadrant, nodes 5 and 6 of the self-equilibrated structure are always in the fourth and first quadrants, respectively, i.e., $270°<\theta_1\leqslant 360°$ and $360°<\theta_1\leqslant 450°$ are satisfied. Figure 4 shows the triangles on the top plane when $\theta_1=60°$. As seen from the figure, the string 9 connecting nodes 4 and 6 is short, and the angle between the strings 7 and 8 connecting pairs of nodes (4, 5) and (5, 6), respectively, is very small for all cases. Figure 5 shows a geometry realization for $\theta_1=80°$. Its bars 2 and 3 connecting pairs of nodes (2, 5) and (3, 6) contact with each other. Such contact always occurs in Case 1. So the structures in Case 1 are not reasonable.

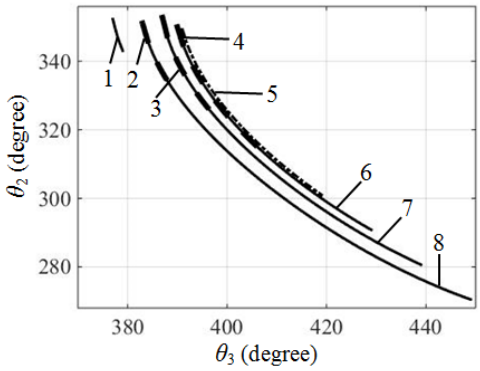

Fig. 3. Variations of θ_2 with respect to θ_3 for Case 1; 1: θ_1=20°, 2: θ_1=30°, 3: θ_1=40°, 4: θ_1=50°, 5: θ_1=60°, 6: θ_1=70°, 7: θ_1=80°, 8: θ_1=90°.

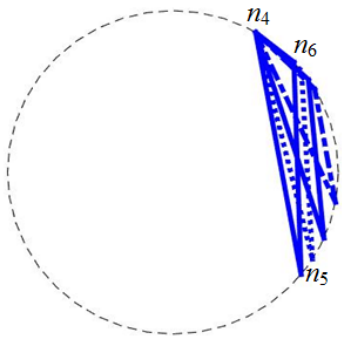

Fig.4. Triangles on the top plane when θ_1=60°.

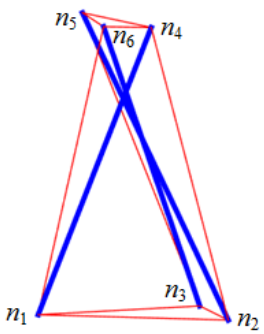

Fig.5. Geometry realization when θ_1=80°.

5. Properties of tensegrity units in Case 2

5.1. Configurations

In Case 2 with $90°<\theta_1\leqslant 180°$, variations of θ_2 and θ_3 are shown in Fig. 6 when θ_1 is varied from 91° to 180°. As seen from the figure, the ranges of θ_3 becomes larger when θ_1 is increased. It has been found in further analysis that increase of $\theta_1\in[90°, 180°]$ always leads to larger range of θ_3; however when θ_1=180°, the range of θ_3 is reduced substantially. It is also seen that the range of θ_2 becomes larger slightly when θ_1 is increased from 91° to 160°; however, it becomes smaller when θ_1 is increased beyond 160°.

For Case 2 where node 4 is located in the second quadrant, it is seen from the values of θ_2 and θ_3 that node 6 is located in the first or fourth quadrant, while node 5 is located in the fourth quadrant. Figure 7 shows the top triangles when θ_1=140°, θ_2=280°and θ_3=140°, respectively. Contrary to Case 1, the top triangles in Case 2 have moderately large angles and edge lengths.

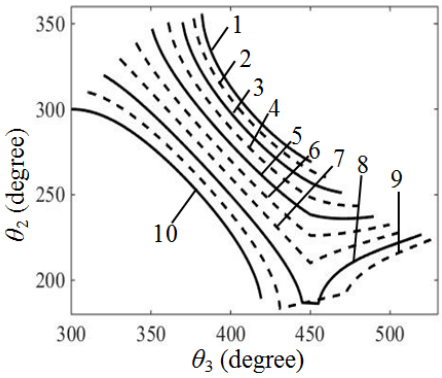

Fig. 6. Variations of θ_2 and θ_3 with respect to θ_1 in Case 2 ; 1: θ_1=91°,2: θ_1=100°,3: θ_1=110°,4: θ_1=120°, 5: θ_1=130°, 6: θ_1=140°, 7: θ_1=150°, 8: θ_1=160°, 9: θ_1=170°, 10: θ_1=180°.

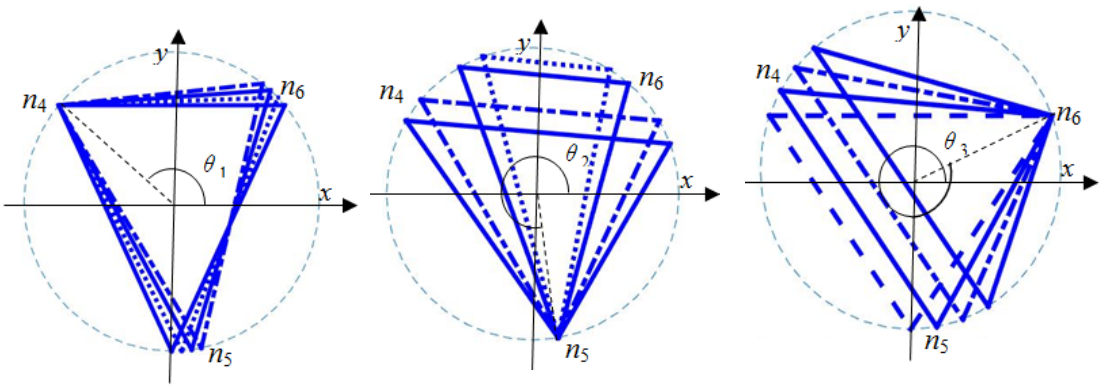

(a) (b) (c)

Fig. 7. Triangles on the top plane; (a) θ_1=140°, (b) θ_2=280°, (c) θ_3=80°.

We fabricated a model for Case 2 with θ_1=160°, θ_2=272°and θ_3=387° as shown in Fig. 8; in the physical model, the angles are measured as θ_1=160°, θ_2=276° and θ_3=387°, which are close to the analytical results. Thus, allowing some fabrication and installation errors, the analytical results have been verified.

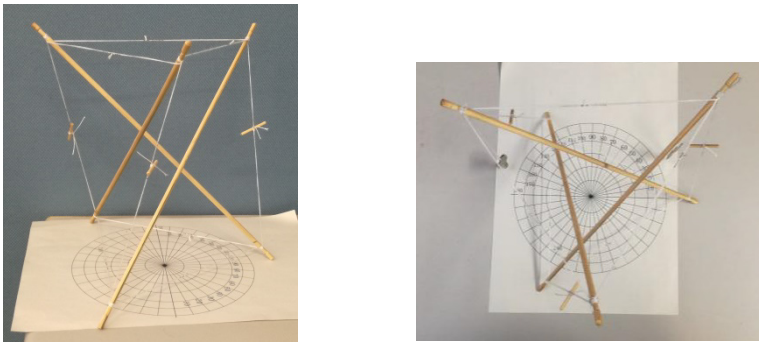

(a) (b)

Fig. 8. A self-equilibrium configuration when θ_1=160°; (a) diagonal view, (b) top view.

In Case 2, the configurations when θ_1=150° are special such that their top triangles are always isosceles triangles as shown in Fig. 9. Figure 10 shows a physical models for θ_1=150°, where top angle of the isosceles triangle is equal to 40°.

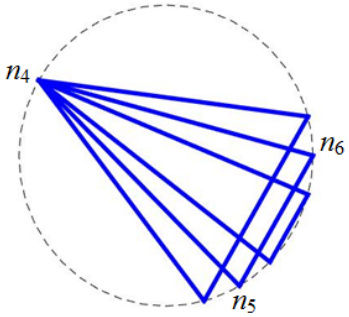

Fig.9. Triangles on the top plane when θ_1=150°.

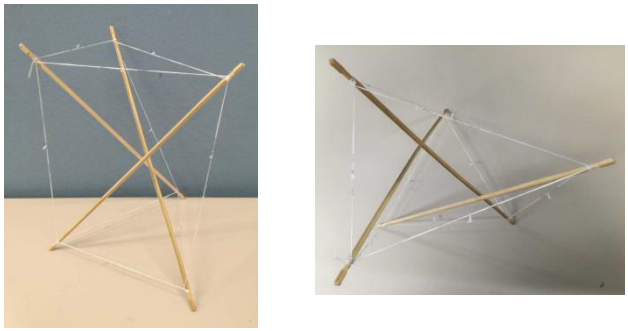

Fig.10. A physical models when θ_1=150°.

5.2. Force densities and internal forces

Eqs. (4)-(6) can be applied to obtain force densities of the members. Since the absolute values of force densities of bars and declining strings are always the same, all of the six force densities are not required to be analyzed. The remaining four force densities are the ratios of force densities of strings to those of the bars. Here θ_1 is assigned as 160° to investigate characteristics of force densities and internal forces of the structure, and then discussions in its range are presented.

Figure 11 shows variations of force densities with respect to θ_3 when θ_1=160°. With increase of θ_3 , q_4 and q_8 decrease, q_7 and q_9 increase, q_5 and q_6 increase first and then decrease. When θ_3=321° , q_4 and q_8 reach their maximum values, while q_5, q_6, q_7 and q_9 are minimum. The maximum of q_8 is 74.47, and the minimum of q_5 and q_6 are equal to 0.001. Distribution of force densities is very uneven. With increase of

θ_3, uneven distribution is improved gradually. When θ_3 approaches 390°, difference among the force densities becomes minimum. Then, with increase of θ_3, difference among the force densities begins to become larger and larger.

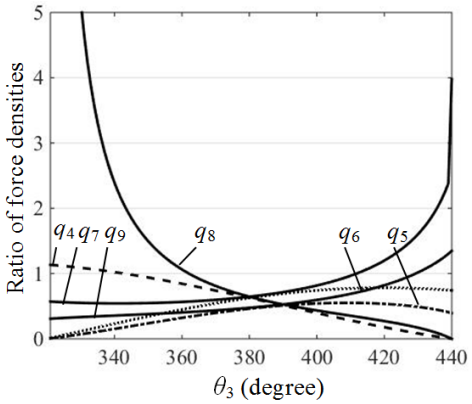

Fig.11. Variations of force densities with respect to θ_3.

Figure 12 shows variations of internal forces with respect to θ_3 when θ_1=160°. As seen from Fig. 12, with increase of θ_3, F_1 and F_{11} are almost constant, F_2 decreases, F_3 increases, F_{10} and F_{12} decrease first and then increase. When θ_3 approaches its upper and lower limits, difference between internal forces becomes large. Conversely when θ_3 approaches median value of its range, distribution of internal forces becomes uniform.

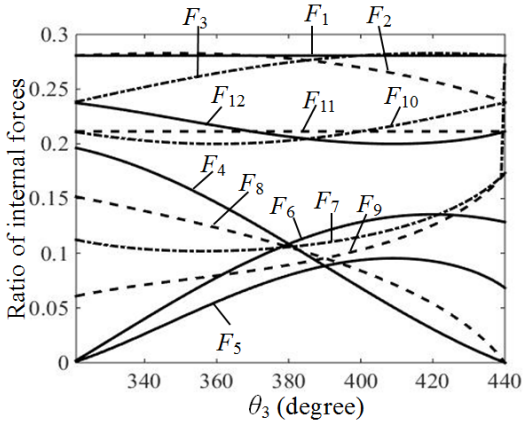

Fig.12. Variations of internal forces with respect to θ_3 when θ_1=160°.

In Fig. 7, the range of θ_3 is [320°, 520°], however the range is [320°, 440°] in Figs. 12 and 13. When θ_3>440°, signs of internal forces of strings are different and there exists no suitable group of internal forces of strings which can be applied to keep the structures at self-equilibrium. Through further analysis, it is found that, the ranges of θ_2 and θ_3 from investigation for configurations are shrunk by analysis for force densities and internal forces in Case 2.

6. Properties of tensegrity units in Cases 3 and 4

In Case 3 with 180°<θ_1≤270°, variations of θ_2 and θ_3 are shown in Fig. 13 when θ_1 varies from 181° to 270°. As seen from Fig. 13, differences between maximum and minimum values of θ_3 are always equal to 118°, when θ_1 is varied from 181° to 240°. The range of θ_3 shrinks drastically for θ_1 from 250° to 270°. It is confirmed from further analysis that difference between maximum and minimum values of θ_3 is constant when θ_1≤242°; the ranges of θ_3≤270° shrinks with the increase of θ_1 when θ_1>242°. Furthermore, it is seen from Fig. 14 that the ranges of θ_2 shrinks when θ_1 is increased. Moreover, when node 4 is located in the third quadrant, node 5 can be located in the third or fourth quadrants, and node 6 can appear in the first,

third or fourth quadrants. Figure 14 shows the top triangles when θ_1=240°, θ_2=250°and θ_3=330°, respectively. The triangles are mostly obtuse triangles.

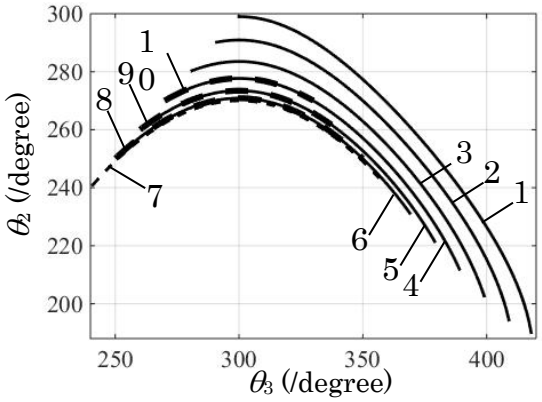

Fig. 13. Variations of θ_2 and θ_3 with respect to θ_1 in Case 3; 1: θ_1=181°, 2: θ_1=190°,3: θ_1=200°, 4: θ_1=210°, 5: θ_1=220°, 6: θ_1=230°, 7: θ_1=240°, 8: θ_1=250°, 9: θ_1=260°, 10: θ_1=270°.

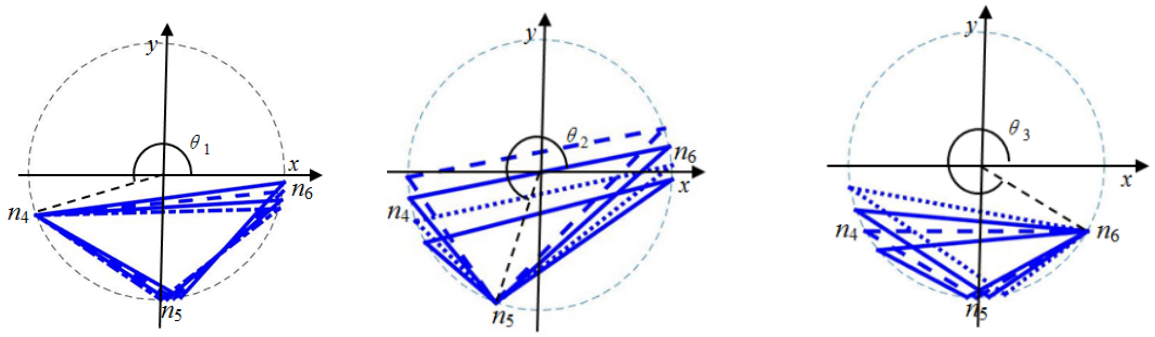

(a) (b) (c)

Fig.14. Triangles on the top plane; (a)θ_1=240°, (b)θ_2=250°, (c)θ_3=330°.

Figure 15 shows a physical model which is set up according to analytical results for θ_1=200°, θ_2=255° and θ_3=360°. In the physical model, the angles are θ_1=202°, θ_2=255° and θ_3=370°, which are a little different from the analytical results due to manufacture and installation error.

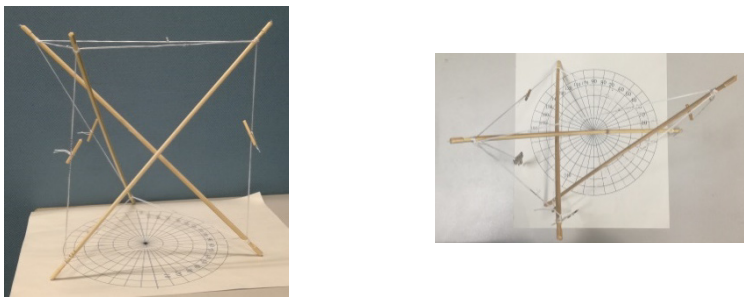

(a) (b)

Fig.15. A self-equilibrium configuration with θ_1=200° for Case 3;
(a) diagonal view, (b) top view.

Internal forces of self-equilibrated structures with θ_1=200° as examples will be applied to investigate characteristics of self-equilibrated structures in Case 3. Figure 16 shows variations of internal forces with respect to θ_3 when θ_1=200°. It is found from Fig.16 that, with increase of θ_3, F_1 and F_{11} are almost constant, F_2, F_4 and F_8 decreases, F_3, F_6 and F_9 increases, F_7, F_{10} and F_{12} decrease firstly and then increase, F_5

increases firstly and then decreases. The range of θ_3 in Fig.13 is from 280° to 399°, while the range in Fig.16 is [320° ,399°]. The range of θ_3 is also shrunk through investigation for internal forces.

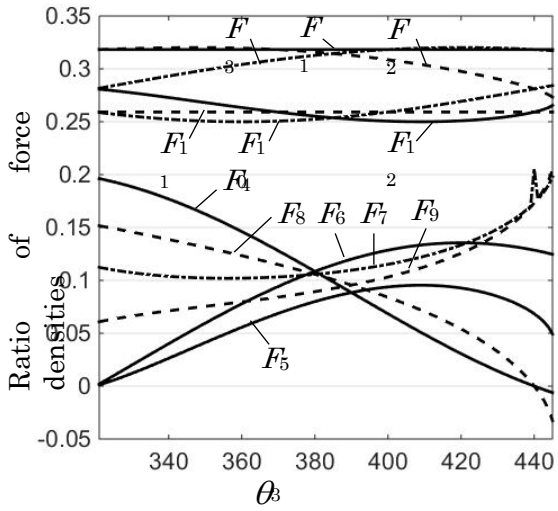

Fig.16. Variations of internal forces with respect to θ_3 when θ_1=200°.

It is found from further analysis that, when θ_1>210°, signs of internal forces of the strings are always wrong and correct group of internal forces of the members cannot be found to keep the structures in Case 3 at self-equilibrium. So there are self-equilibrated structures only when 180°<θ_1≤210° in Case 3. Moreover, when θ_3 approaches its upper and lower limits, uneven distribution of internal forces becomes obvious, which is the same as internal force distribution of the structures in Case 2.

For Case 4 when node 4 stays in the fourth quadrant, there are no configurations satisfying the equilibrium conditions presented in Section 3. It is concluded from analysis results in sections 4, 5 and 6, there are self-equilibrated structures when 90°<θ_1≤210°. Since two 3-bar tensegrity units with θ_1=150° and 210° are symmetric with respect to *xz*-plane, properties of the two units are similar. Therefore, we can apply results for θ_1=150° directly to derive characteristics of configurations with θ_1=210°. Accordingly, analysis for the tensegrity unit with θ_1=210° is not described.

7. Conclusion

In this paper, we investigated the 3-bar prismatic tensegrity unit with a non-equilateral and an equilateral triangles, respectively, on the two end planes, which are parallel with each other. Through analytical solutions of equilibrium equations, we obtain expressions which reflect relations between angles θ_1, θ_2 and θ_3 at the nodes of non-equilateral triangle. The analytical solutions also contain expressions of force densities of all members. Through investigation of the properties in angles and force densities, we obtained the following conclusions:

1)When connectivity of members and nodes of 3-bar tensegrity unit is the same as the well-known 3-bar prismatic tensegrity unit with θ_1=150°, there are self-equilibrated configurations when 90°<θ_1≤210°. When 90°<θ_1<180°, the range of θ_3 increases with increase of θ_1; however, the range of θ_2 increases firstly and then decreases. When 180°<θ_1≤210°, range of θ_2 increases with increase of θ_1; differences between maximum and minimum values of θ_3 is always constant.

2)When θ_1 is given a priori, uneven distribution between internal forces becomes significant as θ_3 approaches its limits. Conversely, when θ_3 approaches the median value of its range, difference between internal forces becomes small.

Acknowledgment

The authors gratefully acknowledge the contribution of National Natural Science Fund of China (Grant Number 51605111, 51675114) and JSPS KAKENHI (Grant Number 15KT0109).

References

[1] X.D. Feng, S.H. Guo. A novel method of determining the sole configuration of tensegrity structures. Mechanics Research Communications, 69 (2015) 66–78.
[2] L.Y. Zhang, Z.L. Zhao, Q.D. Zhang, X.Q. Feng. Chirality induced by structural transformation in a tensegrity: theory and experiment. Journal of applied mechanics, 83 (2016)1-7.
[3] F. Fraternali, G. Carpentieri, A. Amendola. On the mechanical modeling of the extreme softening/stiffening response of axially loaded tensegrity prisms. Journal of the mechanics and physics of solids, 74(2015)136-157.
[4]X. Xu, Y. Luo. Form-finding of nonregular tensegrities using a genetic algorithm. Mechanics Research Communications, 37(2010)85-91.
[5] A. Amendola, G. Carpentieri, M. de Oliveira, R.E. Skelton, F. Fraternali. Experimental investigation of the softening-stiffening response of tensegrity prisms under compressive loading. Composite structures, 117(2014)234-243.
[6] K. Nagase, R.E. Skelton. Network and vector forms of tensegrity system dynamics. Mechanics Research Communications, 59 (2014) 14–25.
[7] A.N. Luo, L.K. Wang, H.P. Liu, Y.Y. Wang, Q.H. Li and X. Li. Analysis of configuration and structural stability of 3-bar tensegrity prism. Journal of harbin institute of technology, 48(2016)82-87.
[8] C. Sultan. Tensegrity: 60 years of art, science, and engineering. Advances in applied mechanics, 43(2009) 69-145.
[9]S. Lee, B. S. Gan, J. Lee. A fully automatic group selection for form-finding process of truncated tetrahedral tensegrity structures via a double-loop genetic algorithm. Composites Part B, 106 (2016) 308-315.
[10] M. Ohsaki, J.Y. Zhang. Nonlinear programming approach to form-finding and folding analysis of tensegrity structures using fictitious material properties. International Journal of Solids and Structures, 69–70 (2015)1–10.
[11] A. Fraddosio, S. Marzano, G. Pavone, M. D. Piccioni. Morphology and self-stress design of V-Expander tensegrity cells. Composites Part B, 115 (2017)102-116.
[12] M. Spisaka, S. Kmet. Shape and Stress Modification of a Chosen Tensegrity System. Procedia Engineering, 190 (2017) 637 – 644.
[13] K. Nagase, T. Yamashita, N. Kawabata. On a connectivity matrix formula for tensegrity prism plates. Mechanics Research Communications, 77 (2016) 29–43.
[14] J.Y. Lu, X. Dong, X.L. Zhao, X.L. Wu, G.P. Shu. Form-finding analysis for a new type of cable–strut tensile structures generated by semi-regular tensegrity. Advances in Structural Engineering, 20(2017)772–783.
[15] H. Liu, J. Geng and A. Luo. Tensegrity configuration method on connecting tensegrity units along their axes. Composite Structure,162(2017)341-350.
[16] A.N. Luo, H.P. Liu, Y.X. Liu. Analyzing the driving method for the ball tensegrity robot. 2016 IEEE International Conference on Robotics and Biomimetics (ROBIO), 12(2016).
[17] Y. Koizumi, M. Shibata, S. Hirai. Rolling Tensegrity Driven by Pneumatic Soft Actuators, 2012 IEEE International Conference on Robotics and Automation RiverCentre, 5 (2012)1988-1993.
[18] W.J. Du, S.G. Ma, B. Li, M.H. Wang and S. Hirai. Dynamic Simulation for 6-strut Tensegrity Robots. Proceeding of the IEEE International Conference on Information and Automation, 7 (2014)870-875.
[19]H.P. Liu, J. Y. Zhang and M. Ohsaki. New 3-bar prismatic tensegrity units. Composite Structures, 184(2018)306-313.
[20] M. Schenk, J. L. Herber, S.D. Guest. Design of a statically balanced tensegrity mechanism. ASME 2006 International Design Engineering Technical Conference & Computers and Information in Engineering Conference, Pennsylvania, USA, 9(2006).
[21] A.G. Tibert and S. Pellegrino. Review of form-finding methods for tensegrity structures. International Journal of Space Structures, 26(2011)241-255.
[22] Maplesoft, Maple 2016 User Manual, 2016.
[23] J.Y. Zhang and M. Ohsaki. Tensegrity Structures: Form, Stability, and Symmetry. Springer, 2015.